Published in Journal of Selected Topics in Quantum Electronics (IEEE) 4, issue , 794-802, 1998
which should be used for any reference to this work

Quantum-Well Intermixing for Fabrication of Lasers and Photonic Integrated Circuits

Daniel Hofstetter, Bernd Maisenhölder, and Hans P. Zappe

***Abstract*— Various applications of quantum-well intermixing, ranging from multiwavelength lasers to complex photonic integrated circuits, are described. The fabrication of these GaAs–AlGaAs-based devices relies on the postgrowth definition of regions with varying bandgap, enabling the manufacture of wavelength shifted modulators and lasers, as well as the integration of transparent waveguides with absorbing lasers and detectors. The impurity-free vacancy-enhanced disordering technique employed, and its integration with existing process technologies, will be presented, and examples of multicolor lasers, wavelength shifted modulators and integrated optical interferometers are shown. These applications yield high-optical functionality using relatively simple process and integration technology.**

***Index Terms*— Interferometers, monolithic integration, multiwavelength lasers, photonic integrated circuits, quantum-well intermixing.**

I. Introduction

OVER THE PAST two decades, quantum-well-intermixing (QWI) techniques have matured from a level of rather academic interest into a versatile tool for the fabrication of numerous optoelectronic devices, such as high-power semiconductor lasers or photonic integrated circuits. Starting with impurity-induced layer disordering [1], a variety of methods, such as vacancy-enhanced disordering (VED) [2], ion-implantation-induced intermixing [3], and laser-assisted disordering [4] have been investigated in many laboratories. While the former is probably the most popular, and has already lead to several commercial products, most of the other techniques are not yet employed in large-scale optoelectronic device manufacturing. The present article will review some of our recent results using VED for the fabrication of lasers, optoelectronic components and photonic integrated sensor circuits, thereby indicating that the technology may be approaching an industrially attractive level of maturity.

The next section will outline some of the intermixing techniques developed and studied in the past and will discuss their potential device applications. We follow this with an in-depth look at one of these methods, vacancy-enhanced disordering, which we have developed and employed for the fabrication of numerous optoelectronic devices and circuits. We conclude with a look at the design, fabrication and performance analysis of multicolor lasers, wavelength shifted modulators and two monolithically integrated optical sensor circuits. The latter structures, complete monolithic sensor microsystems, may be of particular industrial interest as they are small, robust, and capable of being produced by mass-fabrication techniques.

D. Hofstetter was with the Paul Scherrer Institute, 8048 Zürich, Switzerland (now Centre Suisse d'Electronique et de Microtechnique SA, Zürich). He is now with the Xerox Palo Alto Research Center, Palo Alto, CA 94304 USA.

B. Maisenhölder was with the Paul Scherrer Institute, 8048 Zürich, Switzerland (now Centre Suisse d'Electronique et de Microtechnique SA, Zürich). He is now with Balzers Thin Films, 9496 Balzers, Liechtenstein.

H. P. Zappe is with the Centre Suisse d'Electronique et de Microtechnique SA, 8048 Zürich, Switzerland.

II. Summary of Important Intermixing Techniques

The combination of lasers and transparent waveguides on a single epitaxially grown substrate for the fabrication of photonic integrated circuits requires the definition of regions with different bandgap energies. The means to solve this problem can be divided into growth and intermixing approaches. The most popular among the growth methods are selective area growth [5], [6] and etch-and-regrowth on a patterned substrate [7], [8]. The first allows the *simultaneous* epitaxy using different growth rates, and, therefore, the growth of quantum wells with different thicknesses. In contrast, the second uses *subsequent* growth of material with different QW thicknesses.

An alternative approach relies on selective partial intermixing of the QW using impurities [9] or vacancies [10]. During a high-temperature anneal, the QW material intermixes with that of the barrier material, resulting in a change in QW shape and thus transition energies. Key to the applicability of a QWI approach is the ability to selectively define the regions which are to be intermixed and those that are not. The primary advantage of intermixing methods is that they require no epitaxial regrowth and are thus potentially simpler and more cost-effective. In the following, we describe several QWI approaches and means of patterning intermixed and nonintermixed regions.

The first QW intermixing technique to be demonstrated was impurity-induced layer disordering (IILD). In 1981, Laidig *et al.* [1], [11], demonstrated the disordering of an AlAs–GaAs superlattice using Zn as the active species. In these early experiments, a thermal anneal of several hours at temperatures of 600 °C was used. As a result of this process, they found, depending on the anneal conditions, different grades of intermixing in a superlattice. In 1983, lasers with blue-shifted emission wavelengths were fabricated using this technique [12]–[14]. In 1984, stripe geometry QW laser devices using IILD to laterally define the waveguide of a buried heterostructure became available [15]–[17], and one year later, the first

QW laser with transparent facet windows fabricated by IILD was demonstrated [18]. Since then, this intermixing method has been refined, and is now probably the one which is best understood and used for a variety of commercial products; the most prominent of these are high-power semiconductor lasers with disordered facet windows.

Instead of incorporating impurities, such as Si, Mg, or Zn, into the lattice with a diffusion process, one can also use ion implantation. Implantation has the primary advantage of not automatically introducing heavy p- or n-type doping when incorporating the reactive species and of having a greater variety of species available [19]–[21]. On the other hand, the crystal damage due to the high implant energies is not as easily removable as in the case of other material systems such as Si. Both of the above intermixing processes rely on impurity atoms which enhance the Al–Ga self-diffusion by different mechanisms. Although there are still debates about the exact nature of the intermixing processes, the important role of the column-III-vacancies and column-III-interstitials could be confirmed by several experiments and authors [22].

Ten years ago, impurity-free intermixing methods, such as VED, became popular, mainly because they offer the possibility of intermixing without doping, thereby preventing strong free-carrier absorption, and without implantation-induced crystal damage which would otherwise be responsible for scattering loss. The first experiments used an As-rich ambient in a quartz ampoule in order to prevent crystal surface damage by arsenic out-diffusion [23]. In 1988, an evaporated SiO_2 encapsulant to enhance intermixing was demonstrated for the first time [24], [25]. Soon thereafter, other dielectrics such as SiON or Si_3N_4 turned out to be suitable for the purpose of creating vacancies and therefore supporting intermixing. In 1993, some fluorides such as SrF_2 or AlF_3 were discovered to efficiently prevent QWI [26]. These materials allowed the definition of a certain pattern with different bandgap energies, essential for the fabrication of opto-electronic devices. The emerging applications will be discussed in detail in the following section.

While the thermal anneal step in most intermixing techniques is carried out in RTA ovens, there are other approaches which use the absorption of a high-energy laser beam to generate the high temperatures required locally. Although this approach is in general not very different from vacancy-enhanced disordering, there might some benefits in terms of obtaining sharp transitions between intermixed and nonintermixed material. In photonic integrated circuits, this approach may have advantages in reduction of waveguide losses.

III. VED: Technology

For reasons of process simplicity and compatibility with existing fabrication steps, we decided to employ VED for the fabrication of lasers, modulators and, ultimately, complete monolithic optical circuits. As a means of evaluating the efficacy of this approach for generating selectively transparent regions on a single substrate, we first studied the extent of wavelength shift with anneal on simple epitaxially grown substrates, later used for the fabrication of heterostructure lasers.

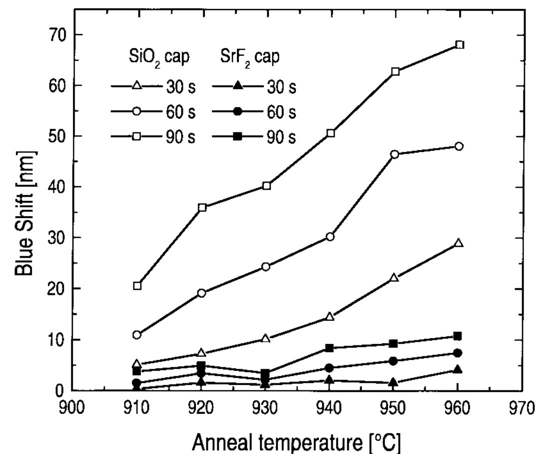

Fig. 1. PL wavelength shift of SiO_2-capped and SrF_2-capped material after VED at different anneal temperatures and anneal times. Excitation of the photoluminescence was accomplished with an argon-ion laser ($\lambda = 488$ nm, $P = 10$ mW) and measured at room temperature.

The epitaxial layer structure used for these first experiments was grown by metal–organic vapor phase epitaxy (MOVPE) on a GaAs substrate (n-doped 10^{18} cm^{-3} Si). An undoped 165-nm-thick $Al_{0.3}Ga_{0.7}As$ waveguide core containing one GaAs QW (7 nm) was sandwiched between a 1.1-μm-thick $Al_{0.8}Ga_{0.2}As$ lower cladding layer (n-doped 1.5×10^{18} cm^{-3} Si) and an 0.85-μm-thick $Al_{0.8}Ga_{0.2}As$ upper cladding layer (p-doped 10^{18} cm^{-3} Mg). A 160-nm-thick highly p-doped (5×10^{18} cm^{-3} Zn) GaAs cap layer completed the structure.

The VED process required that the sample be completely covered with a single layer of either e-beam evaporated SiO_2 or thermally evaporated SrF_2. The fabrication steps to achieve this structure were based on a self-aligned process; this was important because an uncapped GaAs surface experiences a much higher risk of being damaged during RTA than a capped one. After deposition of a 200-nm-thick SiO_2 layer, we photolithographically defined areas to be covered with SrF_2. In these regions, the SiO_2 layer was removed by CF_4 reactive ion etch (RIE). Using the same photoresist mask a second time, we then evaporated a 250-nm-thick SrF_2 layer and patterned it using a liftoff process.

During the subsequent RTA step, group-III-vacancies are generated under the SiO_2-cap but not under the SrF_2-cap. Under SiO_2, the vacancies promote intermixing of Ga atoms in the initially pure GaAs QW with Al atoms of the adjacent $Al_{0.3}Ga_{0.7}As$ core, thereby increasing the Al-content and the energy bandgap of the QW. The final effect is an anneal-temperature-dependent blue-shift of the transition energy, a change manifested in a shift of the photoluminescence (PL) spectrum. Fig. 1 shows the achieved blue-shifts in the PL spectrum as a function of temperature and anneal time. After an RTA of 30-, 60-, and 90-s duration, and at temperatures between 910 °C and 960 °C, we measured blue-shifts of 5–68 nm under the SiO_2-cap and less than 10 nm under the SrF_2-cap, yielding a differential of almost 60 nm. For further processing, both dielectric layers had to be removed: the SiO_2 layer was stripped in a CF_4 plasma and the SrF_2 layer in diluted HCl (HCl/H_2O 1:10, 10 s).

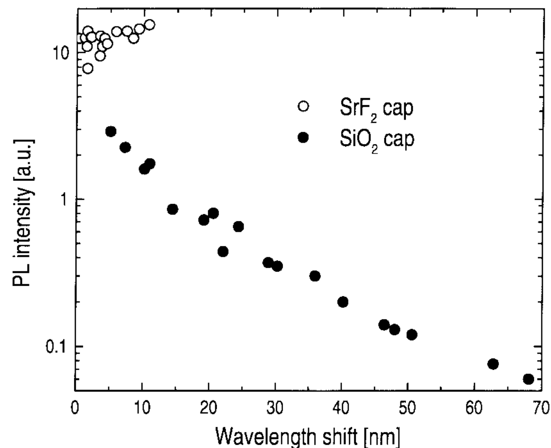

Fig. 2. PL intensity of SiO_2-capped and SrF_2-capped material after VED at different anneal temperatures and anneal times.

In Fig. 2, the PL intensity as a function of the PL shift for both shifted and nominally un-shifted material is shown; it appears that the PL intensity of SiO_2-capped material decreases exponentially with the amount of blue-shift. This phenomenon may occur because of the indirect recombination of electrons and holes via deep interband levels, formed by Ga-vacancies, or by the spilling of carriers from the QW into the barrier region (which is more likely in an intermixed and, therefore, shallow QW). The slight PL intensity increase of the SrF_2-capped material could be due to greater surface roughness causing light scattering into the acceptance angle of the collection optics of the spectrometer.

As a reduction in PL intensity could thus imply a degradation in material quality, we were cautious in the application of intermixing to various devices. For multiwavelength lasers, for example, a blue-shift of only 20 nm was employed, which, according to Fig. 2, leads to only a 30% reduction in PL intensity; the change in laser behavior is discussed in a following section. For the fabrication of photonic integrated circuits, use of the blue-shifted regions was confined to that of passive waveguides, whose performance is not expected to be affected by a degradation in PL efficiency.

The VED approach for selectively promoting a blue-shift in the absorption wavelength can then easily be used to define transparent regions in a waveguide-based optical circuit in QW material; for the sensor applications discussed below, the passive waveguides and couplers were fabricated in regions covered with SiO_2 during anneal, whereas the lasers and photodetectors were defined in the unshifted regions defined by SrF_2. For the multiwavelength lasers, we used both the shifted and the unshifted sections of the material for their fabrication.

IV. Lasers and Electrooptic Devices

We subsequently employed the VED technique for the fabrication of multiwavelength Fabry–Pérot lasers, wavelength shifted modulators and distributed Bragg reflector (DBR) lasers with a nonabsorbing reflector. This broad range of application provided an indication of the flexibility of the VED approach for use in numerous types of optoelectronic devices.

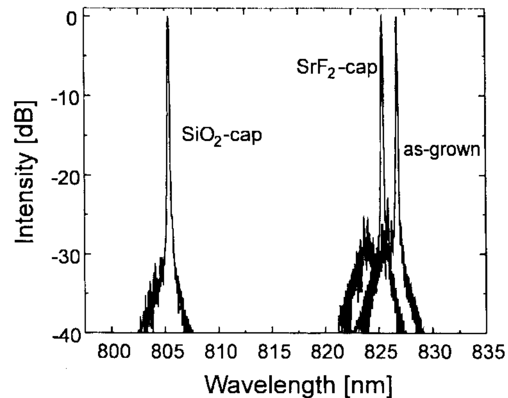

Fig. 3. Emission spectra of representative as-grown, SiO_2-capped and SrF_2-capped Fabry–Pérot lasers.

A. *Multiwavelength Fabry–Pérot Laser Arrays*

The layer structure for the Fabry–Pérot lasers was identical to the one used for the initial intermixing experiments. These lasers consisted of a 4-μm-wide single-mode ridge waveguide which was dry etched to a depth of 100 nm above the waveguide core. Passivation and electrical isolation of the ridge sidewalls was accomplished through a 250-nm-thick PECVD-grown Si_3N_4-layer. After a contact hole etch on top of the ridges, standard p- and n-metal layers were evaporated.

In order to demonstrate the effect of material subject to a VED anneal on laser performance, we fabricated Fabry–Pérot lasers in both the shifted and the unshifted regions of annealed material, as well as in as-grown material [27]. The lasers were 500 μm long and were tested under CW conditions at room temperature. The bars were tested p-side up on a copper heat-sink. The spectra of representative as-grown, SrF_2-, and SiO_2-capped devices are shown in Fig. 3; we see laser emission at wavelengths of 826, 823, and 805 nm. The VED-induced wavelength shifts were thus 3 and 21 nm, for the nominally unshifted and shifted regions, respectively. All lasers emitted light in a single lateral and longitudinal mode with a sidemode suppression of about -20 dB.

The threshold current density of the as-grown laser was 600 A/cm^2 and its slope efficiency 0.52 W/A. In comparison, the SiO_2-capped laser had a lower threshold current density of 500 A/cm^2 while the SrF_2-capped device had a somewhat higher threshold current density of $J_{\rm th} = 700$ A/cm^2. The slope efficiencies of the SiO_2-capped laser (0.42 W/A) and the SrF_2-capped laser (0.36 W/A) were lower than that of the as-grown laser.

The higher threshold current and lower slope efficiency of the SrF_2-capped laser were probably caused by repeated plasma exposure of its contact region during SiO_2 removal, SiO_2 patterning and Si_3N_4 patterning. This was also indicated by the higher threshold voltage of the SrF_2 capped device ($V(I_{\rm th}) = 3.3$ V) when compared to the as-grown and the SiO_2-capped laser ($V(I_{\rm th}) = 2.15$ V). We believe that the unexpected higher threshold current of the as-grown device is caused by a slightly different ridge geometry due to processing variations across the wafer. Pulsed operation of these lasers did not markedly change the threshold currents or the external

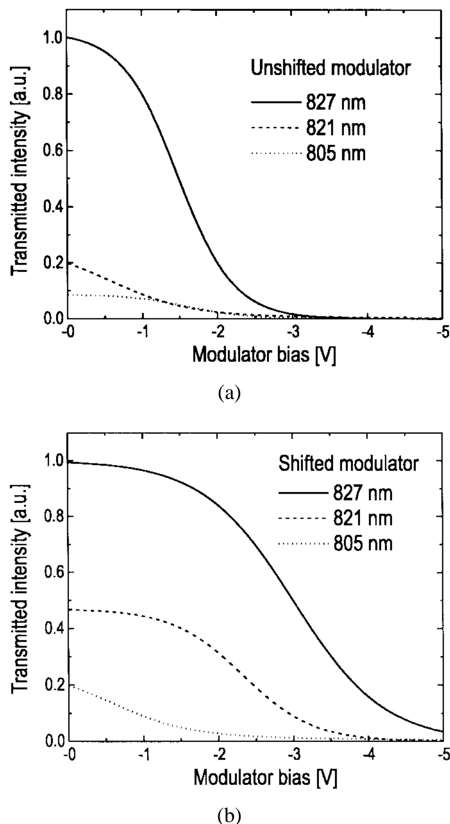

Fig. 4. (a) Extinction curves of QCSE-based unshifted intensity modulators measured for three different excitation wavelengths. (b) Extinction curves of QCSE-based wavelength-shifted intensity modulators measured for three different excitation wavelengths. The absorption edge of this device was blue-shifted by 20 nm.

quantum efficiencies and exhibited similar emission wavelength differences between the devices; this clearly indicates that the wavelength shifts were not due to device heating.

B. Wavelength-Shifted Modulators

Using the same epitaxial layer structure as described above, waveguide-based electroabsorption modulators with different absorption edge wavelengths were fabricated on a single piece of semiconductor; these devices relied on the quantum confined Stark effect [28]. By fabricating modulators in regions shifted and unshifted by VED, the absorption edge could be tuned in wavelength. Since, by the Kramers–Kronig relation, electroabsorption implies electro-refraction, this fabrication-induced wavelength tunability can be advantageously used for the optimization of electrorefractive phase modulators, as will be discussed in more detail below.

The 500-μm-long 4-μm-wide waveguide modulators were tested in bar form on a temperature-controlled chuck. Light from an external-cavity tunable laser was focused onto the cleaved facet using a microscope objective; the transmitted light was likewise imaged through an objective onto a Si photodetector and the signal amplified by lock-in techniques. The modulator transmission was evaluated at wavelengths of 827, 821, and 805 nm.

As can be seen in Fig. 4(a), which corresponds to the extinction curves for an unshifted modulator with an optimum operating wavelength at 830 nm, only the longest wavelength (827 nm) shows appreciable transmission at zero modulator bias. -10-dB modulation depth was achieved at a bias of -2.5 V, and -20 dB at a bias of -3.6 V. For the modulator fabricated in intermixed material, with the extinction characteristics shown in Fig. 4(b), -10-dB modulation depth was reached for -4.3-V modulator bias, and -20 dB was not accomplished. Since the optimum operating wavelength for the shifted modulator was at around 810 nm, its modulator characteristics show considerably higher biases than the unshifted one for a similar degree of extinction. For example, we notice that for the unshifted device and an excitation wavelength of 821 nm, only -1.9-V bias is necessary to achieve 10% of its unbiased transmission, whereas the shifted modulator requires -3.6-V bias for a comparable modulation depth. When comparing the shape of the extinction curves at 827 nm, we realize that the intermixed modulator shows an extinction characteristic dilated along the voltage axis. If we assume a linear relationship between modulator bias and position of the absorption edge, this suggests that the absorption edge changed both wavelength position and shape during the intermixing process. The observation that the absorption edge becomes more gradual in an intermixed QW is consistent with the fact that its depth and shape change from a deep square potential into a more rounded, shallow potential.

For moderate extinction ratios up to 10 dB, which are typical for operation at an excitation wavelength 20 nm above the bandgap wavelength, we expect a chirp $c = \Delta n/\Delta k$ on the order of $c = 2$, resulting in an electrorefractive phase shift of $\pi/4$ for a 500-μm-long modulator. Phase shifts of this order will be used in the interferometer devices which will be presented in the next section.

C. DBR Laser

In the following paragraph, we describe some important device characteristics of a two-section DBR laser with a nonabsorbing grating. This laser was fabricated using the same layer structure as described in the previous experiments. The pumped section of the laser was fabricated in an area of the chip not subject to a bandgap shift during VED, while the Bragg reflector was etched into the shifted, thus nonabsorbing, region. A device containing this kind of DBR laser and coupled to a passive waveguide and a photodetector, is presented in Fig. 5. The use of a grating recess allowed accurate vertical placement of the grating [33]; this recess was dry etched to within 150 nm of the active region, leaving an accurately defined layer for the Bragg reflector. The holographically defined third-order grating had a period of 375 nm, 1:1 line-to-space ratio and 100-nm depth. By varying the thickness of the buffer layer between grating and waveguide core, the coupling coefficient could be fine-tuned within a reasonable range.

Performance evaluation of discrete DBR lasers was carried out CW at room temperature. Maximum output power was 5 mW from the cleaved facet, threshold current was 26 mA ($J_{\mathrm{th}} = 1.3$ kA/cm^2) and slope efficiency was on the order

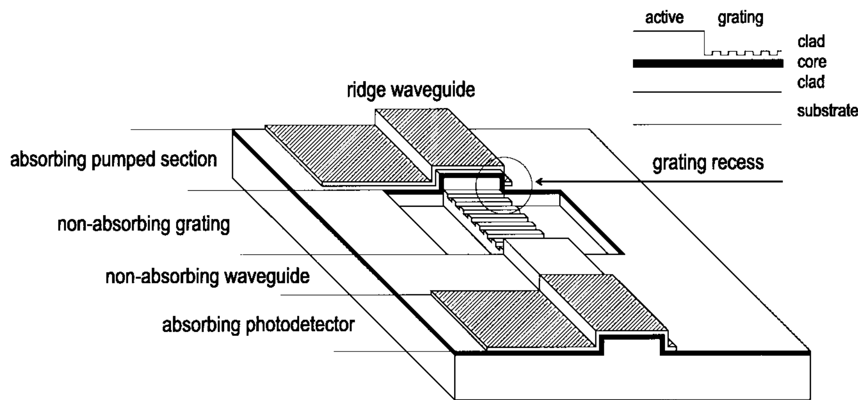

Fig. 5. Schematic picture of a two-section DBR laser with a recessed nonabsorbing grating and monolithically integrated with a transparent waveguide section and a photodiode.

of 0.21 W/A. The subthreshold laser spectrum ($I = 0.96 \times I_{\mathrm{th}}$) shown in Fig. 6 allowed an approximate experimental evaluation of the grating coupling coefficient by determining the stopband-width of the reflection curve. The value obtained was 120 cm^{-1}, which compares reasonably well with the calculated value of 100 cm^{-1}. The spectrum above threshold, measured at $I = 2.3 \times I_{\mathrm{th}}$, is shown as an inset of Fig. 6; it is single longitudinal mode with a primary emission peak at $\lambda = 820$ nm and a sidemode suppression ratio of 27 dB. High-resolution spectral measurements and detailed near-field studies indicated that the laser operated with a single transverse mode. Self-heterodyne measurements of the laser spectrum gave a spectral linewidth of 500 kHz. The primary emission peak could be continuously temperature-tuned between 15 and 35 °C with a temperature tuning coefficient of 0.06 nm/°C.

Although these DBR lasers were fabricated with nonabsorbing gratings, their threshold current density did not greatly improve with respect to those devices which had absorptive gratings. However, one has to take into account that these nonabsorbing gratings were designed to reflect only 40% whereas the absorptive gratings reflected close to 100%. In the former case, we therefore had a nonabsorbing, but only moderately reflecting laser mirror, while in the latter, we dealt with an absorptive but also highly reflective mirror. Since we observed similar threshold current densities for both types of DBR lasers, these two mechanisms balanced each other for our device configurations.

The reason for the use of two different grating strengths was related to the fact that the DBR laser with the intermixed grating section was designed for driving an optical integrated circuit whereas the device with the absorbing grating was a discrete prototype device. The prototype was designed without the intermixing process and thus to have a minimal penetration depth of the light into the unpumped DBR section; a long unpumped section would result in a high absorption loss and a high threshold current density. For the laser as part of the optical integrated circuit, in which the intermixing step was included, a longer DBR section could be made and the reflectance could be reduced; a reflectance of 40% was sufficient to allow efficient lasing and left the remaining 60% for coupling into the optical circuit.

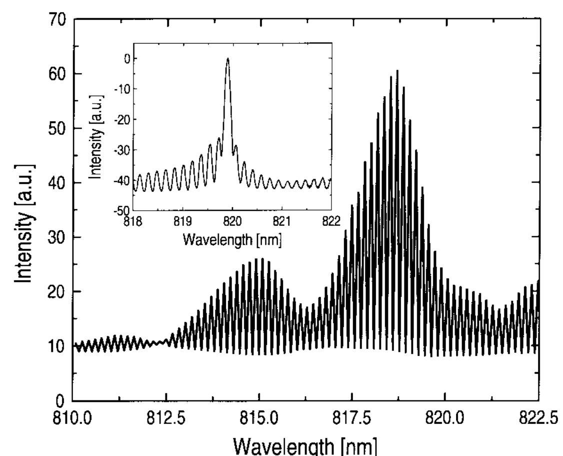

Fig. 6. Optical spectrum of a DBR laser with a 500-μm-long pumped and a 130-μm-long grating section driven at $I = 0.96 \times I_{\mathrm{th}}$. The inset shows the spectrum of the same device above threshold at $I = 2.3 \times I_{\mathrm{th}}$.

V. Photonic Integrated Circuits

Using the above DBR laser process and VED, we then built different kinds of photonic integrated circuits. In this last section, we will discuss three rather advanced circuits; namely a DBR laser with integrated photodetector, and two monolithically integrated interferometric sensors.

A. Integration: Laser, Waveguide, and Photodetector

Numerous approaches have been developed for the integration of a laser with an optical circuit; these include evanescent coupling between waveguides and emitting regions (requiring an additional impedance matching layer and regrowth) [29], [30], butt coupling between laser and photodetector (needing a mirror dry etch technique) [31] or the use of surface emitting lasers and photodiodes (requiring high-quality dry-etched mirrors) [32]. For the present work, the use of a simplified, single-growth-step, two section DBR laser, described above [33], [34], represents an attractive solution with respect to both process compatibility and feedback stability for an integrated interferometer.

To test the suitability of the DBR lasers and the VED technique for bandgap shifting described above, a simple optical

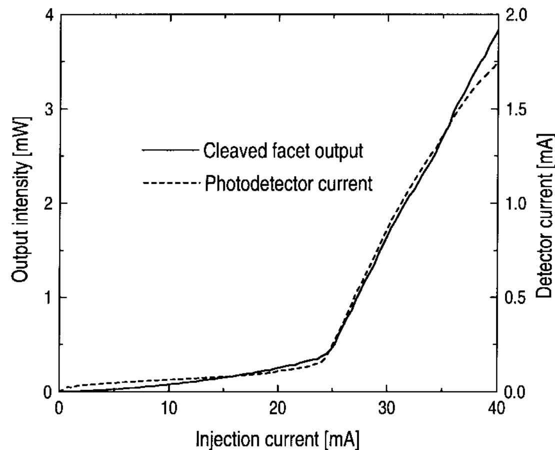

Fig. 7. Cleaved facet optical output power and photodetector current versus laser injection current of a DBR laser monolithically integrated with a transparent waveguide and an absorbing photodetector.

(a)

(b)

Fig. 8. (a) Micrograph of a DMI for optical displacement measurement with direction determination. On the far left, the contact pads for the pumped DBR section and the photodiodes are shown. The small rectangle to the right of the DBR laser contact pad is the grating recess with the grating. Above and below the word MOD, there are two contact pads for the phase modulators. Two directional couplers are visible above and below the word DC 550 and (b) micrograph of an MZI which is configured as a refractometer. The three contact pads for DBR laser, phase modulator, and photodiode are wired to the far right side of the device. The two parallel ridge waveguides with the phase modulator in one interferometer arm are separated by only 50 μm and are visible just below the PSI logo.

circuit consisting of 500-μm-long pumped laser sections, 130-μm-long nonabsorbing DBR reflectors, 570-μm-long transparent waveguides, and 500-μm-long absorbing photodiodes was fabricated. The entire chip, 1700-μm-long, was traversed by a single 4-μm-wide waveguide and is shown schematically in Fig. 5.

Similar to the DBR laser with a nonabsorbing grating section, we fabricated the grating and the transparent waveguide of this device in an area subject to VED while the pumped laser section and the photodetector were built in nonintermixed areas of the wafer. As shown in Fig. 7, we simultaneously measured the cleaved facet output power with an external photodetector and the output power from the grating side of the laser with the integrated photodetector; for current values up to 35 mA, the two curves follow each other closely. Above this current level, the integrated photodetector saturates, mainly because no reverse bias voltage was applied. This operating condition was chosen because the resistance parallel to the reverse biased photodiode is about 5 kΩ and thus leakage currents were relatively high. The performance of integrated photodiodes was found to be very similar to as-grown material photodiodes. They typically exhibit a high responsivity of >0.6 A/W, implying >90% quantum efficiency.

In order to estimate the optical absorption loss of waveguides fabricated in the intermixed areas of the device, we measured the cleaved facet output on the grating side before and after having removed photodetector and transparent waveguide. Since the performance of a DBR laser is adversely affected by the presence of a cleaved facet on the grating side, we evaporated a single-layer antireflection coating on each cleaved facet. By this method, waveguide losses of 30 dB/cm were determined. This number is similar to the absorption loss measured on waveguides fabricated from as-grown material when using an excitation wavelength 20 nm red-shifted to the absorption edge of the material. The fact that intermixed and as-grown waveguides show comparable absorption losses when measured under similar conditions indicates that the intermixing process does not introduce significant excess defect levels; these would appear as a greatly enhanced absorption loss.

B. Interferometer Design and Characterization

The optical sensor circuits we describe in the following two paragraphs are a double Michelson interferometer (DMI) and a Mach–Zehnder interferometers (MZI); both of them are shown as microscope photographs in Fig. 8(a) and (b). The DMI devices included one DBR laser, two photodetectors, two Y-couplers, two directional couplers, and two phase shifters. The ridge width of the waveguides was 3 μm and all curve radii were 500 μm, while the MZI devices consisted of a DBR laser, two Y-couplers, one photodetector, one phase modulator and one dielectric waveguide. The passive waveguides were fabricated in the areas with intermixed quantum wells and had, because of the relatively small bandgap difference of 45 meV between intermixed and nonintermixed sections, an absorption loss of 35–45 dB/cm. Since the total waveguide length did not exceed 3 mm, this relatively high absorption loss was not overly detrimental for interferometer performance. The total chip lengths were 2.6 mm for DMI's and 5 mm for MZI's.

Both the pumped laser section and photodetectors were fabricated in the nonintermixed, and thus absorbing, areas of the chip and had a length of 500 μm each. The length of the nonabsorbing DBR grating section was 200 μm; here, we used a third order grating with a period of 380 nm, a depth of 160 nm and 1:1 line-to-space ratio. A 70-nm thin buffer layer between the bottom of the grating and the waveguide core resulted in a calculated grating coupling coefficient of 100 cm^{-1}; this gave the desired grating reflection coefficient of about 95%. The left cleaved facet of the interferometer served as the second laser mirror.

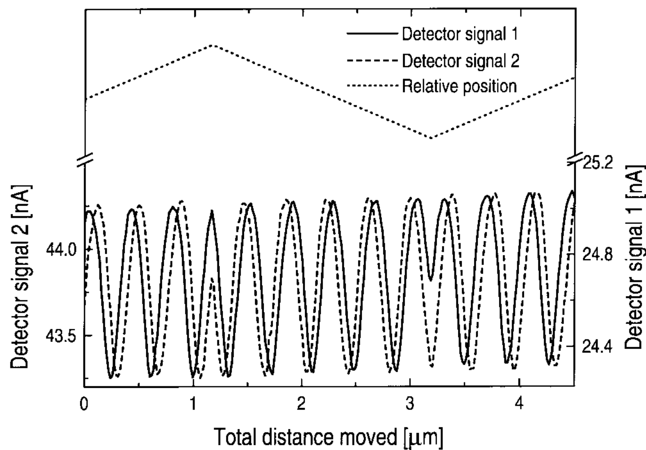

Fig. 9. The two detector currents of the double Michelson interferometer for 3.5-cm mirror distance and 67% mirror reflectance showing the two interference signals. As shown by the position graph, direction changes occurred at 1.2 and 3.2 μm.

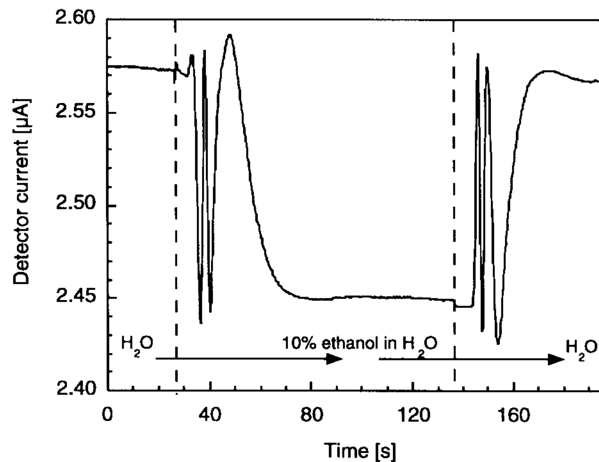

Fig. 10. Interferometer signal versus time for an MZI. At t_1, the analyte was switched from A to B, and at t_2, it was switched back from B to A. The phase shift is 5π in both directions.

C. Position Sensor Based on DMI

These interferometer chips were tested in bar form and were temperature-stabilized to within ± 50 mK using a thermoelectric cooler. The measurement beam, collimated by an external GRIN lens (pitch $= 0.23$), was directed onto a semitransparent, 67% reflecting mirror through which the reflected beam position could be observed by a CCD camera. Observation was necessary to adjust the beam properly into autocollimation. The semitransparent mirror was fixed to a piezo-driven, gimbal-mounted holder with which the measurement distance could be varied between 3 and 45 cm. With this arrangement, we were able to produce a movement with periodically ($T = 60$ s) changing direction; this back-and-forth-type of movement was necessary to check the interferometer's ability to recognize the movement direction.

The DBR lasers in this circuit operated at a current level of 60 mA and a reverse voltage of -12 V was applied to the photodetectors. The length of the phase shifters was 340 μm, which gave a one-pass phase shift of $\pi/16$ when driven at -12-V bias voltage. Fig. 9 presents the result of an interferometric measurement with a DMI at a mirror distance of 3.5 cm. Two changes of movement direction are clearly visible in the figure: one at 1.2 μm and another at 3.2 μm. One interference fringe corresponds to a mirror movement of one half of the measurement wavelength, namely 410 nm. Due to thermal fluctuations on the chip, a noise current with an amplitude of about 20 pA was seen in the detector current, such that the signal noise corresponded to about 5% of the output signal amplitude. A more comprehensive study of the measurement resolution and some noise issues appeared elsewhere [35].

By measuring the response of a photodetector which was connected to a DBR laser via a straight 1.6-mm-long waveguide, we could estimate the waveguide loss in the intermixed areas to be on the order of 40 cm^{-1}. Although this number might look quite large, it did not affect the performance of these interferometers.

D. Refractometer Experiments Using a MZI

The fabrication of these MZI devices differs from the previous device insofar that we used a three QW active region instead of a single QW, and that the waveguide in the sensor pad region consisted of a Ta_2O_5 on SiO_2 dielectric waveguide. The first of these changes was made in order to enlarge the available phase shift of the phase modulator for possible phase-shifting interferometry; this was at the cost of a slightly higher threshold current density of the DBR laser. The second one was required in order to increase the sensitivity, which is defined as the partial derivative of the effective index in the sensor pad region with respect to a cover refractive index change. For performing the refractometric measurements, a flow cell was placed on top of the chip which allowed simultaneously a flow of the analyte liquid across the sensor pad and making electrical contact to the laser, modulator and detector.

Fig. 10 shows the detector signal upon switching analyte A to B at time t_1 and back from B to A at t_2. Analyte A was deionized water ($n_{\mathrm{A}} = 1.3273$), analyte B a solution of 10 vol.% ethanol in water ($n_{\mathrm{B}} = 1.3325$), so that the refractive index difference $\Delta n = n_{\mathrm{B}} - n_A$ was $\Delta n = 0.0052$. The associated phase shift was measured to be $\Delta\Phi = 5\pi$ which corresponds to the associated refractive index change.

The resolution of this interferometer chip was determined by measuring the detector signal of the Mach–Zehnder interferometer drift with the measurement cell placed on top of the MZI with a continuous flow of analyte A. Using a linear fit, the phase drift was determined to be 39 mrad/min, which corresponds to a refractive index resolution of 1.3×10^{-5} for a measurement period of 1 min.

By assuming that approximately 10% of the total power from the cleaved facet mirror (0.5 mW) being emitted from the grating side of the DBR laser, measuring a signal of 2.5 μA at the photodetector, and assuming 0.5-A/W conversion efficiency in the photodetector, we can estimate the waveguide loss to be approximately 40 cm^{-1}. This result is entirely consistent with the result obtained with the DMI and loss measurements on intermixed waveguides.

VI. Conclusion

We have shown that, within the last decade, QWI techniques have evolved into a versatile tool in III–V-semiconductor device fabrication. We presented multiwavelength lasers and monolithically integrated optical sensors fabricated by VED. The latter are single chip devices which can perform either contactless optical displacement measurements or refractometry experiments. They consist typically of a DBR laser, detectors, modulators, and a combination of III–V and dielectric waveguides. We have shown that even rather complex devices combining optically active and passive components can be fabricated without epitaxial regrowth given that QW intermixing technology is readily available.

Acknowledgment

The authors are grateful to J. E. Epler, M. Moser, and H. P. Schweizer for crystal growth; P. Riel, D. Jeggle, and A. Vonlanthen for processing assistance; Y. Salvadé for laser linewidth measurements; and R. Dändliker of the University of Neuchâtel, K. Dransfeld of the University of Konstanz, H. W. Lehmann, and M. T. Gale for their generous support.

References

[1] W. D. Laidig, N. Holonyak, Jr., M. D. Camras, K. Hess, J. J. Coleman, and R. L. Thornton, "Disorder of an AlAs–GaAs super-lattice by impurity diffusion," *Appl. Phys. Lett.,* vol. 38, no. 10, pp. 776–778, 1981.

[2] J. Beauvais, S. G. Ayling, and J. H. Marsh, "Los-loss extended cavity lasers by dielectric cap disordering with a novel masking technique," *IEEE Photon. Technol. Lett.,* vol. 4, pp. 372–373, 1993.

[3] G. F. Redinbo, H. G. Craighead, and J. M. Hong, "Proton implantation intermixing of GaAs/AlGaAs quantum wells," *J. Appl. Phys.,* vol. 74, no. 5, pp. 3099–3102, 1993.

[4] C. J. McLean, A. McKee, G. Lullo, A. C. Bryce, R. M. De La Rue, and J. H. Marsh, "Quantum well intermixing with a spatial selectivity using a pulsed laser technique," *Electron. Lett.,* vol. 31, no. 15, pp. 1285–1286, 1995.

[5] K. Yamaguchi, K. Okamoto, and T. Imai, "Selective area growth of GaAs by metalorganic chemical vapor deposition," *Jpn. J. Appl. Phys.,* vol. 24, pp. 1666–1671, 1985.

[6] D. Trommer, "Photonic integration on InP," in *Proc. ECIO'95,* Delft, The Netherlands, 1995, pp. 93–98.

[7] D. Remiens, B. Rose, M. Carre, and V. Hornung, "CaInAsP/InP integrated ridge laser with a butt-joined transparent optical waveguide fabricated by single-step metalorganic vapor-phase epitaxy," *J. Appl. Phys.,* vol. 68, pp. 2450–2453, 1990.

[8] V. Hornung, D. Remiens, D. Robein, A. Gloukhian, and M. Carre, "Simple approach for monolithic integration of DFB laser and passive waveguide," *Electron. Lett.,* vol. 27, pp. 1683–1685, 1990.

[9] R. L. Thonton, J. E. Epler, and T. L. Paoli, "Monolithic integration of a transparent dielectric waveguide into an active laser cavity by impurity-induced disordering," *Appl. Phys. Lett.,* vol. 51, pp. 1983–1985, 1987.

[10] S. Bürkner, M. Maier, E. C. Larkins, W. Rothemund, E. P. O'Reilly, and J. D. Ralston, "Process parameter dependence of impurity-free interdiffusion in GaAs/$\mathrm{Al}_x\mathrm{Ga}_{1-x}$As and $\mathrm{In}_y\mathrm{Ga}_{1-y}$As/GaAs multiple quantum wells," *J. Electron. Mater.,* vol. 24, no. 7, pp. 805–812, 1995.

[11] N. Holonyak, Jr., W. D. Laidig, M. D. Camras, J. Coleman, and P. D. Dapkus, *Appl. Phys. Lett.,* vol. 39, pp. 102–104, 1981.

[12] M. D. Camras, M. Holonyak, Jr., R. D. Burnham, W. Streifer, D. R. Scifres, T. L. Paoli, and C. Lindström, "Wavelength modification of $\mathrm{Al}_x\mathrm{Ga}_{1-x}$As/GaAs quantum well heterostructure lasers by layer interdiffusion," *J. Appl. Phys.,* vol. 54, pp. 5637–5641, 1983.

[13] K. Meehan, N. Holonyak, Jr., R. D. Burnham, T. L. Paoli, and W. Streifer, "Wavelength modification ($\Delta h\omega$ 10–40 meV) of room temperature continuous wave quantum well heterostructure laser diodes by thermal annealing," *J. Appl. Phys.,* vol. 54, pp. 7190–7191, 1983.

[14] K. Meehan, J. M. Brown, P. Gavrilovic, N. Holonyak, Jr., R. D. Burnham, T. L. Paoli, and W. Streifer, "Thermal-anneal wavelength modification of multiple-well p-n $\mathrm{Al}_x\mathrm{Ga}_{1-x}$As/GaAs quantum well lasers," *J. Appl. Phys.,* vol. 55, pp. 2672–2675, 1984.

[15] K. Meehan, L. M. Brown, N. Holonyak, Jr., R. D. Burnham, T. L. Paoli, and W. Streifer, "Stripe-geometry AlGaAs/GaAs quantum-well heterostructure lasers defined by impurity-inducing disordering," *Appl. Phys. Lett.,* vol. 44, no. 7, pp. 700–702, 1984.

[16] K. Meehan, P. Gavrilovic, N. Holonyak, Jr., R. D. Burnham, and R. L. Thornton, "Stripe-geometry $\mathrm{Al}_x\mathrm{Ga}_{1-x}$As/GaAs quantum well heterostructure lasers defined by Si-diffusion and impurity-induced disordering," *Appl. Phys. Lett.,* vol. 46, no. 1, pp. 75–77, 1985.

[17] D. G. Deppe, K. C. Hsieh, N. Holonyak, Jr., R. D. Burnham, and R. L. Thornton, "Low-threshold disorder-defined buried-heterostructure $\mathrm{Al}_x\mathrm{Ga}_{1-x}$As/GaAs quantum well lasers," *J. Appl. Phys.,* vol. 58, no. 12, pp. 4515–4520, 1985.

[18] R. L. Thornton, D. F. Welch, R. D. Burnham, T. L. Paoli, and P. S. Cross, "High-power (2.1 W) 10-stripe AlGaAs laser arrays with Si-disordered facet windows," *Appl. Phys. Lett.,* vol. 49, no. 23, pp. 1572–1574, 1986.

[19] Hirayma, Y. Suzuki, and H. Okamoto, "Ion-species dependence of interdiffusion in ion-implanted GaAs/AlAs superlattice," *Jpn. J. Appl. Phys.,* vol. 24, pp. 1498–1502, 1985.

[20] J. J. Coleman, P. D. Dapkus, C. G. Kirkpatrick, M. D. Camras, and N. Holonyak, Jr., "Disorder of an AlAs/GaAs superlattice by silicon implantation," *Appl. Phys. Lett.,* vol. 40, pp. 904–906, 1982.

[21] B. C. De Cooman, C. B. Carter, and J. R. Ralston, "$\mathrm{Al}_{1-x}\mathrm{Ga}_x$As/GaAs superlattice disordering by ion-implantation and diffusion: A TEM study of mechanisms," in *SPIE Proc., Advanced Processing of Semiconductor Devices,* S. D. Mukherjee, Ed. Bellingham, WA: SPIE, 1987, vol. 797, pp. 185–196.

[22] D. G. Deppe and N. Holonyak, Jr., "Atom diffusion and impurity-induced layer disordering in quantum-well III–V-semiconductor heterostructure," *J. Appl. Phys.,* vol. 64, no. 12, pp. R93–R113, 1988.

[23] L. J. Guido, N. Holonyak, Jr., K. C. Hsieh, R. W. Kaliski, W. E. Plano, R. D. Burnham, R. L. Thornton, J. E. Epler, and T. L. Paoli, "Effects of dielectric encapsulation and As overpressure on Al–Ga interdiffusion in $\mathrm{Al}_x\mathrm{Ga}_{1-x}$As/GaAs quantum well heterostructures," *J. Appl. Phys.,* vol. 61, no. 4, pp. 1372–1379, 1987.

[24] J. D. Ralston, S. O'Brien, G. W. Wicks, and L. F. Eastman, "Room-temperature exciton transitions in partially-intermixed GaAs/AlGaAs superlattices," *Appl. Phys. Lett.,* vol. 52, no. 18, pp. 1511–1513, 1988.

[25] E. S. Koteles, B. Elman, P. Melman, J. Y. Chi, and C. A. Armiento, "Quantum well shape modification using vacancy generation and rapid thermal annealing," *Opt. Quantum Electron.,* vol. 23, pp. S779–S787, 1991.

[26] J. Beauvais, J. H. Marsh, A. H. Dean, A. C. Bryce, and C. Button, "Suppression on bandgap shifts in GaAs/AlGaAs quantum wells using strontium fluoride caps," *Electron. Lett.,* vol. 28, no. 17, pp. 1670–1672, 1992.

[27] D. Hofstetter, H. P. Zappe, J. E. Epler, and P. Riel, "Multiple wavelength Fabry–Pérot lasers fabricated by vacancy-enhanced quantum well disordering," *Appl. Phys. Lett.,* vol. 67, pp. 1978–1980, 1995.

[28] D. A. B. Miller, D. S. Chemla, T. C. Damen, A. C. Gossard, W. Wiegmann, T. H. Wood, and C. A. Burrus, "Band-edge electroabsorption in quantum well structures: The quantum confined Stark effect," *Phys. Rev. Lett.,* vol. 53, no. 22, pp. 2173–2176.

[29] R. J. Deri, W. Doldissen, R. J. Hawkins, R. Bhat, J. B. D. Soole, L. M. Schiavone, M. Seto, N. Andreadakis, Y. Silberberg, and M. A. Koza, "Efficient vertical coupling of photodiodes to InGaAsP rib waveguides," *Appl. Phys. Lett.,* vol. 58, pp. 2749–2751, 1991.

[30] K.-Y. Liou, U. Koren, E. C. Burrows, M. Oron, B. J. Miller, M. Young, G. Raybon, and C. A. Burrus, "Operation of integrated InGaAsP/InP optical amplifier-monitoring detector with feedback control circuit," *IEEE Photon. Technol. Lett.,* vol. 2, pp. 878–880, 1990.

[31] P. Vettinger, M. K. Benedict, G.-L. Bona, P. Buchmann, E. C. Cahoon, K. Dätwyler, H.-P. Dietrich, A. Moser, H. K. Seitz, O. Voegeli, D. J. Webb, and P. Wolf, "Full-wafer technology—A new approach to large-scale laser fabrication and integration," *IEEE J. Quantum Electron.,* vol. 27, pp. 1319–1331, 1991.

[32] C.-H. Chen and S.-C. Lee, "Monolithic integration of an AlGaAs/GaAs surface emitting laser diode and a photodetector," *Appl. Phys. Lett.,* vol. 59, pp. 3592–3594, 1991.

[33] D. Hofstetter, H. P. Zappe, J. E. Epler, and J. Söchtig, "Single-growth-step GaAs/AlGaAs distributed Bragg reflector lasers with holographically-defined recessed gratings," *Electron. Lett.,* vol. 30, pp. 1858–1859, 1994.

[34] D. Hofstetter, H. P. Zappe, and J. E. Epler, "Ridge waveguide DBR lasers with nonabsorbing grating and transparent integrated waveguide," *Electron. Lett.,* vol. 31, pp. 980–982, 1995.

[35] D. Hofstetter, H. P. Zappe, and R. Dändliker, "Displacement measurements with monolithically integrated GaAs/AlGaAs-based Michelson interferometers," *J. Lightwave Technol.,* vol. 10, pp. 663–671, Aug. 1997.

Daniel Hofstetter was born in Zug, Switzerland, in 1966. In 1993, he received the Dipl. Phys. ETH degree in physics from the Swiss National Institute of Technology (ETH) with his diploma thesis entitled "CO-laser photoacoustic spectroscopy of fatty acid vapors," which was carried out under the supervision of Prof. F. K. Kneubühl at the Infrared Laboratory of the ETH in Zurich. He received the Ph.D. degree in physics from the University of Neuchâtel, in 1996, for his dissertation entitled "Monolithically integrated displacement sensor for optical displacement measurement."

After an apprenticeship as an Electrical Mechanic at Landis & Gyr in Zug (1982–1986), he worked for the same company as a Physics Technician (until 1988). He is currently working as a post-doctoral Researcher at the Xerox Palo Alto Research Center in Palo Alto, CA. He is active both in InGaN–GaN laser research and in integration of multicolor lasers for scanning applications.

Bernd Maisenhölder was born in Stuttgart, Germany, in 1966. In 1990/1991, he spent half a year as a Fulbright scholar at the Louisiana State University, Baton Rouge, LA. He received the M.S. degree in physics from the University of Konstanz, Germany, in 1994 and the Ph.D. degree in the field of III–V integrated optics for chemical and biochemical sensing applications from the Paul Scherrer Institute in Zurich, Switzerland.

After he finished his doctoral research in 1997, he joined the R&D department of the thin-film business unit of Balzers Corporation in Liechtenstein. He is currently involved in the development of submicrometer gratings for integrated optical grating couplers and their various applications.

Hans P. Zappe was born in Paris, France, in 1961. He received the B.S. and M.S. degrees in electrical engineering from the Massachusetts Institute of Technology (MIT), Cambridge, MA, in 1983, and the Ph.D. degree in electrical engineering from the University of California, Berkeley, in 1989.

He has worked for IBM in Essex Junction, VT, and the Fraunhofer Institute for Applied Solid State Physics in Freiburg, Germany, at first on silicon VLSI and subsequently on III–V optics. He is presently at the Centre Suisse d'Electronique et de Microtechnique SA (CSEM) in Zurich, Switzerland, leading projects on the development of photonic integrated circuits and custom semiconductor lasers for sensor and metrology applications. He also teaches postgraduate courses in integrated optics and lasers at the Neu-Technikum, Buchs, Switzerland.